Defect and Diffusion Forum, vol. 120, 73-90, Advances in Mass and Thermal Transport in Engineering Materials III, ISSN print 1012-0386. https://s3.wp.wsu.edu/uploads/sites/893/2023/02/DSL_238-2022-a.pdf

Diffusional Relaxation of Quadrupole Interactions of ^{111}In/Cd probes in $IrIn_3$ and related phases having $FeGa_3$ Structure

Randal L. Newhouse[1,a], Prastuti Singh[1,b], Matthew O. Zacate[2,c] and Gary S. Collins[1,d *]

[1]Dept Physics and Astronomy, Washington State University, Pullman, WA 99163, USA
[2] Dept Physics, Geology and Engineering Technology, Northern Kentucky University, Highland Heights, KY 41099, USA

[a]randynewhouse@gmail.com, [b]singhprastuti@gmail.com, [c]zacatem1@nku.edu, [d]collins@wsu.edu

*corresponding author

Keywords: diffusion, jump-frequency, nuclear quadrupole interaction, nuclear relaxation, vacancy diffusion mechanism, site-preference.

Abstract. Nuclear relaxation caused by diffusion of ^{111}In/Cd probe atoms was measured in four phases having the tetragonal $FeGa_3$ structure (tP16) using perturbed angular correlation spectroscopy (PAC) and used to gain insight into diffusion processes in phases having more than one diffusion sublattice. The three indide phases studied in this work have two inequivalent and interpenetrating In-sublattices, labeled In1 and In2, and nuclear quadrupole interactions were resolved for probes on each sublattice. The phases are line-compounds with narrow field-widths. Diffusional relaxations, fitted using an exponential damping *ansatz*, were measured at the two opposing boundary compositions as a function of temperature. "High" and "low" relaxation regimes were observed that are attributed to In-poorer and In-richer compositions, under the reasonable assumption that the atomic motion occurs via an indium-vacancy diffusion mechanism. Relaxation was observed to be greater for tracer atoms starting on In2 sites in the indides immediately following decay of ^{111}In into ^{111}Cd, which is attributed to a preference of daughter Cd-tracer atoms and/or indium vacancies to occupy In1 sites. Activation enthalpies for relaxation are compared with enthalpies for self-diffusion in indium metal.

Introduction

Bulk diffusion reflects the average behavior of a diffusing tracer species. For diffusion on a cubic sublattice, the bulk diffusivity D is simply proportional to the mean jump frequency w via

$$D = \frac{1}{6} f \ell^2 w, \qquad (1)$$

in which ℓ is the jump-distance and f is a correlation-factor [1]. The classic method for determining D is by measuring the concentration profile of a tracer element penetrating into a host. Alternatively, application of microscopic methods sensitive to individual atomic jumps can provide greater insight into diffusion processes [1]. One such method is perturbed angular correlation of gamma-rays, or PAC, a hyperfine method used to measure interactions between the quadrupole moment of an excited-state tracer nucleus and the electric field gradient (efg) at the nucleus produced by nearby electric charges. PAC was first applied to study diffusion of a tracer in a seminal study on $LaIn_3$ in 2004 [2]. $LaIn_3$ has the cubic $L1_2$, or Cu_3Au, structure, and there are three inequivalent orientations of the local efg at tracer atoms on the In-sublattice. Each jump of a tracer on the In-sublattice leads to *reorientation* of the efg by 90-degrees without change in magnitude. Jumps that occur during the lifetime of the excited nuclear state then lead to

decoherence of the nuclear quadrupole perturbation that is observable as damping of the quadrupole perturbation function. Using a stochastic model, the dynamically damped perturbation can be fitted to obtain the mean jump-frequency w of the tracer atom at the measurement temperature [2]. Measurements over a range of temperature can be fitted using an Arrhenius form to obtain the jump-frequency activation enthalpy. Studies have been made of diffusional relaxation in many other $L1_2$ phases [3,4,5,6,7,8] as well as in phases having other structures [9,10,11]. While PAC is restricted to a small number of radioisotopes having favorable nuclear decay properties, one can complete an entire series of measurements at different temperatures using a single sample.

A different kind of diffusional relaxation occurs in tetragonal crystals if there are jumps between inequivalent sites, but when all efgs are axial and aligned along the tetragonal axis. One then has fluctuations in *magnitudes* of the efgs without reorientation of efg tensors. A recent study was made on a series of phases having the common Al_4Ba structure [12], in which there are two inequivalent Al-sublattices, labeled Al1 and Al2, with the local structure such that atoms on Al1 sites jump to Al2 sites and atoms on Al2 sites jump to Al1 sites. Thus, there is a change in magnitude of the efg in each jump. At low temperature, one observes static quadrupole interactions for ensembles of tracer probes on each of the two sublattices. With increasing temperature, the magnitudes of the efgs fluctuate between two values, leading to motional averaging of the two quadrupole interaction frequencies. Eventually, the two dynamically averaged frequencies merge into a single frequency at a temperature such that the mean jump-frequency between the two sublattices equals the difference between the static quadrupole interaction frequencies. The physical situation is analogous to frequency-shift keying (FSK) in communications, with shifts occurring with each jump of the tracer atoms [12].

In this paper is considered nuclear relaxation for tracer atoms in phases having the tetragonal $FeGa_3$ (tP16) structure [13], including $IrIn_3$, $RhIn_3$, $RuIn_3$, $CoGa_3$ and $CoIn_3$. The crystal-structure, studied in detail by U. Haeussermann et al. [13], is shown in Fig 1. There are two inequivalent In-sites, labeled In1 and In2 according to the numbers of atoms of each type per formula unit. In the figure, In1 sites are at the centers of cubes of In2-atoms.

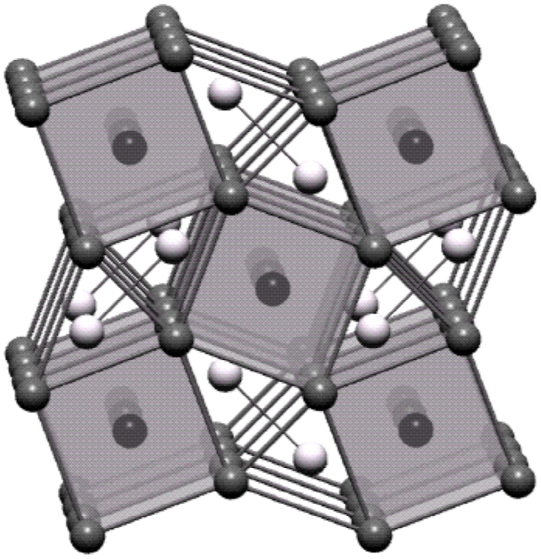

Figure 1. Crystal structure of $IrIn_3$. Transition-metal atoms (white) form dumbells. There are two inequivalent sublattices of indium atoms (black) with a 1:2 ratio of sites. Along the tetragonal axis, as pictured, In1 atoms are at centers of slightly distorted cubes of In2 atoms (shaded). As described in the text, tracer atoms on In1 sites can jump to any of their eight surrounding In2 sites, whereas tracers on In2 sites can jump either to four nearby In1 sites, to four In2 sites along cube edges, to two In2 atoms in layers vertically above and below, or to one In2 site along the very short diagonal across the neighboring rhombus. Figure reproduced with permission from [13].

This system offers a more complex diffusion scenario than is found in either $L1_2$ or Al_4Ba phases since tracer atoms occupy two inequivalent sublattices and each jump within or between the sublattices leads to reorientation and/or change in magnitude of the local efg tensor. A previous study of relaxation in $FeGa_3$ using PAC [14] showed a strong site-preference of the tracer impurities for Ga2 sites (In2-type), with no occupation of Ga1 sites. The lack of occupation of Ga1

sites by In-atoms, where they would be surrounded by eight Ga2-neighbors, is attributed to a repulsive interaction between In and Ga atoms; indeed, In and Ga form no intermetallic compounds [15] and the solubility limit of In in solid-Ga has been found using PAC to be at a mole-fraction of 10^{-11} [16]. This leads to a more restricted diffusion scenario than in the indides because tracers on Ga2 sites can only jump to other Ga2 sites. The measurements reported here are mostly from the dissertation research of Randal Newhouse [17]. Below are sample-preparation methods, measurements and results, and a discussion.

Sample Preparation

Studies were made on samples of $IrIn_3$, $RhIn_3$, $RuIn_3$, $CoGa_3$ and $CoIn_3$ phases. Relaxation was observed in four of the five phases, but not in $CoIn_3$ because no relaxation was evident below the peritectic temperature of 490°C at which the phase disappears [18]. Samples were made by arc-melting metals of purity greater than 99.9% together under argon in a small bell-jar, with trace amounts of carrier-free ^{111}In activity (mole-fraction of order 10^{-10}).

The phases all appear as line-compounds in binary phase diagrams. In previous studies it has been found that site-preferences and jump-frequencies can be highly sensitive to composition near a stoichiometric composition [19]. Accordingly, it became routine practice in this laboratory to prepare and study pairs of samples with mean compositions just beyond boundaries of the phase of interest (e.g., 24.8 and 25.2 at.% for a 1:3 phase). This leads to two-phase mixtures in which the volume fraction of the phase of interest is dominant and its composition is anchored at the boundary composition. For example, consider diffusion in a 1:3 compound such as $IrIn_3$ taking place via an indium-vacancy mechanism, with hypothetical boundary compositions of 24.8 and 25.2 at.% of Ir. Since mole-fractions of vacancies vary monotonically with composition, the mole-fraction of vacancies on the In-sublattice will be greater at the 25.2 at.% Ir composition than at the 24.8 at.% composition. This in turn leads to a greater jump-frequency in the Ir-rich (In-poor) sample. While the mean composition of the sample remains in the two-phase field on either side of the phase field of the phase of interest, the equilibrium composition remains locked at the corresponding boundary composition. This stabilizes measurements against a gradually changing vacancy mole-fraction, such as might be caused by evaporation of a host element in measurements at high temperature.

While preparation of the Fe and Co phases was routine, it turned out to be difficult to obtain homogeneous indide phases of Ir, Rh and Ru immediately after melting and solidification, owing to their extremely high melting temperatures, respectively 2719, 2237 and 2607 K. Indeed, the indium metal with which the transition-metals react boils at 1 atm at 2282 K, making it difficult to achieve a molten mixture of the constituent elements. However, samples were found to become homogeneous within the first ~2 days of two-week measurements at 400-800 °C. Indirect evidence from analysis of the PAC measurements appears to clearly indicate which samples were poorer or richer in indium than the stoichiometric 75:25 composition ratio, but that evidence often conflicted with nominal compositions from masses of the melted metals, as detailed in the *Appendix*.

Perturbed Angular Correlation of Gamma Rays

PAC spectroscopy makes use of the angular correlation between successive nuclear radiations. The tracer isotope used in this study is ^{111}In/Cd. The parent ^{111}In isotope (mean life 4d) decays by electron-capture to an excited state of ^{111}Cd, which subsequently decays to the 247 keV PAC level.

Following electron-capture, two gamma-rays are emitted in sequence. Existence of an angular correlation and directional anisotropy in the emissions of the two gamma-rays allows one to monitor the time-evolution of the nuclear spin of intermediate 247 keV state of the daughter probe caused by interaction of the quadrupole moment in the local electric field-gradient (efg). The

interaction leads to "precessions" that can be detected by measuring coincidence spectra of the second gamma-ray at fixed angles of 180° and 90° relative to the first. Typical magnitudes of electric field-gradients in solids lead to quadrupole interaction frequencies of order 10 MHz. Because the PAC level is long-lived (120 ns), the nuclear spin can precess through large angles, allowing good resolution of quadrupole interaction frequencies for probe atoms on different sites. Measurements were made using four-counter spectrometers with BaF_2 scintillating crystals [20]. After subtracting accidental coincidences, coincidence spectra $W(\theta,t)$ measured at relative angles of 180° and 90° were algebraically combined to obtain the total quadrupole perturbation function $G_2^{tot}(t)$ (see [20])

$$G_2^{tot}(t) = \frac{2}{3}\frac{1}{A_2\gamma_a}\frac{W(180,t)-W(90,t)}{W(180,t)+2W(90,t)}, \qquad (2)$$

in which A_2= -0.18 is the angular anisotropy of the 171-245 keV gamma-cascade of ^{111}Cd and $\gamma_a \approx 0.7$ is an angular-attenuation factor that accounts for the finite solid-angles subtended by the detectors from the sample. For more information about methods see refs. [21, 20]. While the chemistry of the parent ^{111}In-probe determines its site-preference, measurements of quadrupole interactions are made on the 247 keV level of the ^{111}Cd daughter-probe. Thus, the observed nuclear relaxation is caused by atomic jumps of Cd-daughter solutes.

The experimental perturbation function in eq. 2 is a sum of perturbation functions for ensembles of probe atoms in each occupied lattice location, multiplied by their respective site-fractions. The intermediate, or PAC, level has spin-5/2, from which each perturbation function has the following *static* form, with three frequency-harmonics at low temperature,

$$G_2^{static}(\omega_1,\eta,t) = s_0(\eta) + \sum_{n=1}^{3} s_n(\eta)\cos\left[\omega_n(\omega_1,\eta)t\right]. \qquad (3)$$

Here, ω_1 is the fundamental observed frequency-harmonic, frequency-harmonics ω_2 and ω_3 are functions of the fundamental frequency and electric field-gradient asymmetry parameter η ($0 \le \eta \le 1$), and the amplitudes s are functions of η. In the special case when η=0 (called axial symmetry), $\omega_n = n\omega_1$ and $s_{0,1,2,3} = 1/5$, 13/35, 10/35, 5/35, which in this work is the case for probe atoms on site In1. Probe atoms on site In2 (or Ga2) have lower symmetry and three frequency harmonics ω_1, ω_2 and ω_3= ω_1+ ω_2, with $\omega_1 < \omega_2 < 2\omega_1$. In fair approximation, $\omega_2 \approx (2-\eta)\omega_1$. Table 1 lists quadrupole interaction frequencies measured at 500°C for the five phases as well as for $CoIn_3$, in which nuclear relaxation was not detected below the 480°C peritectic temperature at which the phase becomes unstable.

Table 1. Quadrupole interactions at 500°C, The amplitude-ratio was 1:2 for sites 1 and 2 in all indides. In the two gallides, ^{111}In impurity atoms occupied only Site 2.

Phase	Site 1		Site 2	
	ω_1 (Mrad/s)	η	ω_1 (Mrad/s)	η
$FeGa_3$	-	-	447.3(6)	0.846(1)
$CoGa_3$	-	-	329.1(5)	0.560(2)
$IrIn_3$	383.5(3)	(0)	384.5(3)	0.605(1)
$RhIn_3$	328.0(4)	(0)	338.7(3)	0.574(1)
$RuIn_3$	393.1(3)	(0)	499.1(3)	0.898(1)
$CoIn_3$ (400°C)	292.8(1)	(0)	273.4(2)	0.638(1)

Defect and Diffusion Forum, vol. 120, 73-90, Advances in Mass and Thermal Transport in Engineering Materials III, ISSN print 1012-0386. https://s3.wp.wsu.edu/uploads/sites/893/2023/02/DSL_238-2022-a.pdf

Dynamical averaging of quadrupole perturbation functions

As temperature increases, probe atoms start to jump to neighboring sites having efg's differing in orientation or magnitude. Once the mean residence-time of the probe decreases to the point that it is comparable to the decay time of the PAC level (τ= 120 ns), the PAC perturbation function becomes "damped" due to decoherence of the nuclear precessions.

In this slow-fluctuation regime, damping can be empirically fitted by multiplying the static perturbation-function observed at low temperature by an exponentially decaying function,

$$G_2^{dynamic}(\lambda,\omega_1,\eta,t) = \exp(-\lambda t) G_2^{static}(\omega_1,\eta,t)\,. \qquad (4)$$

Here, λ is the relaxation frequency, proportional to the mean jump-rate of the PAC probe atoms.

Elementary situations occur when each jump leads to the unique change in the efg, either through change in magnitude or orientation of the efg at the nuclear site. Consider, first, probes jumping on the majority sublattice in the $L1_2$ crystal structure [2]. There, the efg reorients by 90-degrees in each jump on that sublattice, without change in magnitude. In the slow-fluctuation regime, in which the jump-rate is less than the quadrupole-interaction frequency, the dynamically averaged perturbation function is given by eq. 4 with relaxation frequency λ equal to the mean jump-frequency [2].

Consider, next, probes jumping between sites in two sublattices that have collinear efgs of different magnitudes. Here, jumps lead to a motional averaging of two static quadrupole-interaction frequencies, with mean-frequencies merging into a single frequency when the jump-rate exceeds the difference in static quadrupole-interaction frequencies. This situation is realized in phases having the common Al_4Ba structure, with a study recently submitted for publication [12]. For this scenario, the perturbation function can be fitted using a weighted sum of eq. 4 for the two frequencies, and in the slow-fluctuation regime where λ_i is proportional to the total jump rate out of site *i*,

$$G_2^{tot}(t) = a_0 + f_1 \exp(-\lambda_1 t) G_2^{static}((\omega_1)_1,\eta_1,t) + f_2 \exp(-\lambda_2 t) G_2^{static}((\omega_1)_2,\eta_2,t)\,. \qquad (5)$$

For $FeGa_3$-type phases studied here, there are multiple, microscopic jump processes, with tracer atoms jumping among both In1 and In2 sites, with many possible changes in magnitudes and orientations of efgs. Unlike in the Al_4Ba phases, the local efgs at Ga2 or In2 sites are not axially symmetric and are not in general orientationally equivalent, and efg components for In2 sites are, moreover, not parallel to tetragonal crystal axes, so that jumps even among type-2 sites lead to reorientation of the efg. Thus, relaxation in these phases has a mixture of relaxation effects observed in both $L1_2$ and Al_4Ba structures. However, spectra can still be fitted using eq. 5, with relaxation factors λ_i for site *i* proportional to the total jump rate away from the site.

The situation for gallide phases $FeGa_3$ and $CoGa_3$ is simpler than for the indide phases because ^{111}In/Cd probes only occupy Ga2-sites, so that there are no jumps to Ga1-sites. A sophisticated analysis was carried out of measurements on $FeGa_3$ that entailed calculating efg's at the different Ga2 sites using DFT methods and then constructing a dynamical matrix to simulate and fit PAC spectra [14]. It was found that the relaxation factor in that work could be expressed in terms of two microscopic jump-frequencies, of which one could be fitted well, and was found to be equal to roughly one-half of the observed empirical relaxation frequency, while the other could not be determined with precision due to uncertainty in efg orientation that could not be resolved by DFT. For further detail, see [14]. Because both In1 and In2 sites are occupied in the indide phases and

there are more possible jump pathways to consider than there was for FeGa3, even larger uncertainty in fitted parameters are expected through use of a microscopic model; therefore, measurements in this paper were analyzed using only the empirical damping *ansatz*.

The efg relaxation rate derives from the underlying physical jump-rates. Qualitatively, the empirical relaxation frequency λ is proportional to an average microscopic frequency $< w >$; that is, $\lambda \cong a < w >$, with a proportionality coefficient a of order unity, perhaps within a factor of 4.

Identifying Quadrupole Interaction Signals with Sites

Figure 2 compares fourier transforms of time-domain PAC spectra for ^{111}In/Cd probes in $FeGa_3$ and $RuIn_3$ at room temperature. The $FeGa_3$ frequency spectrum (top) exhibits only one quadrupole-interaction triplet signal with fundamental frequency ω_1= 477 Mrad/s and η = 0.895. The $RuIn_3$ spectrum exhibits two signals, one having fundamental frequency ω_1= 503 Mrad/s and η= 0.901 and the other ω_1= 394 Mrad/s and exhibiting frequency harmonics in proportion to 1:2:3 characteristic of axial symmetry (η ~ 0.0). The amplitude of the 503 Mrad/s signal is approximately double that of the 394 Mrad/s signal, as expected for signals on In2 and In1 sites, respectively. The local symmetry of In1 sites is expected to be axial. The closeness of the 477 and 503 fundamental frequencies and the similar values of η indicate that In-probes only occupy In2(Ga2) sites in $FeGa_3$. In $CoGa_3$, In-probes similarly occupy only Ga2 sites, whereas in all the indides, In2 and In1 sites are occupied with a 2:1 ratio of amplitudes, as shown for $RuIn_3$.

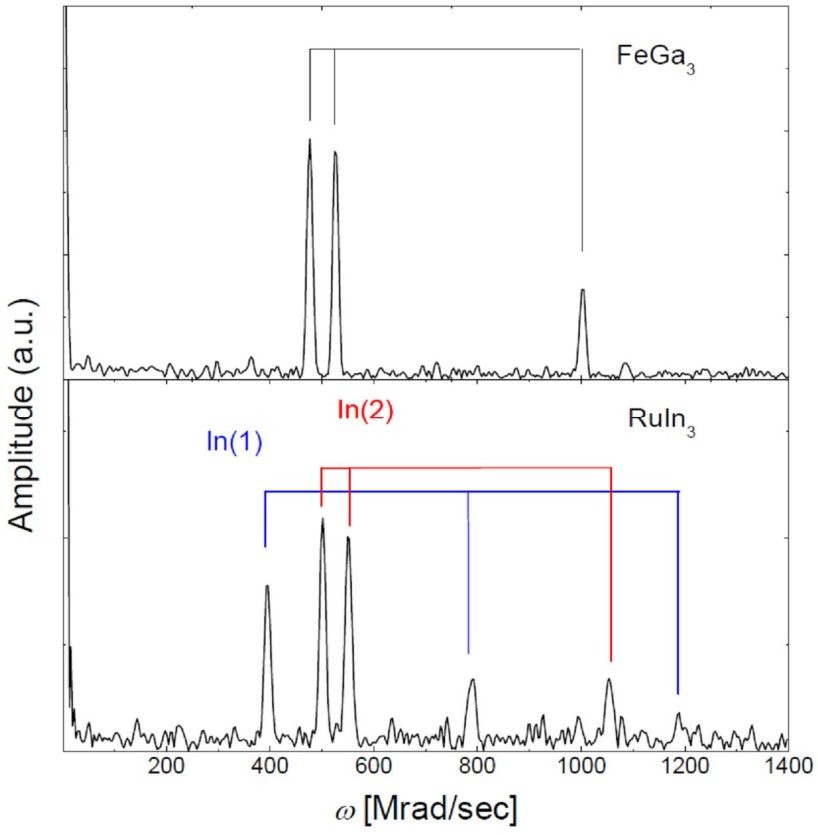

Fig. 2. Frequency spectra for ^{111}In/Cd probes in $FeGa_3$ and $RuIn_3$ at room temperature. Triplet-patterns for $RuIn_3$ are identified with probes on In1 and In2 sites. By comparing the two spectra, the signal for $FeGa_3$ is seen to arise from probes on Ga2 sites, with none detected on Ga1 sites.

We now present results for each of the four phases studied.

Defect and Diffusion Forum, vol. 120, 73-90, Advances in Mass and Thermal Transport in Engineering Materials III, ISSN print 1012-0386. https://s3.wp.wsu.edu/uploads/sites/893/2023/02/DSL_238-2022-a.pdf

$CoGa_3$

The temperature dependence of the static quadrupole interaction and onset of dynamical relaxation is illustrated in Fig. 3 from spectra of $FeGa_3$ measured at three temperatures. Spectra for $CoGa_3$ look essentially the same.

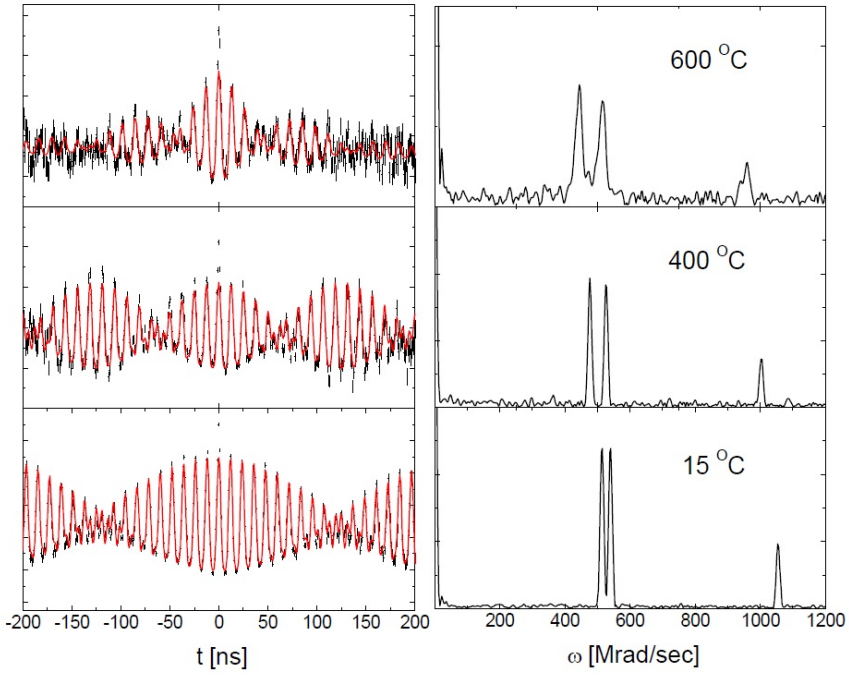

Fig. 3. Time-domain and frequency spectra of $FeGa_3$. With increasing temperature, there is a large decrease of η from a value close to one. Large amplitudes of the ω_1 and ω_2 harmonics produce the beating pattern. Dynamical relaxation at 600°C is evident as exponential attenuation of the static perturbation function or as broadening of peaks in the frequency spectrum. "Double-sided" spectra such as this display independent data at apparently negative times.

Spectra for $CoGa_3$ were measured over the range 450-700°C and fitted with exponential relaxation according to eq. 4. An Arrhenius plot of relaxation frequencies is shown in Fig. 4 and exhibits well-defined thermal activation of the relaxation with enthalpy 0.88(2) eV.

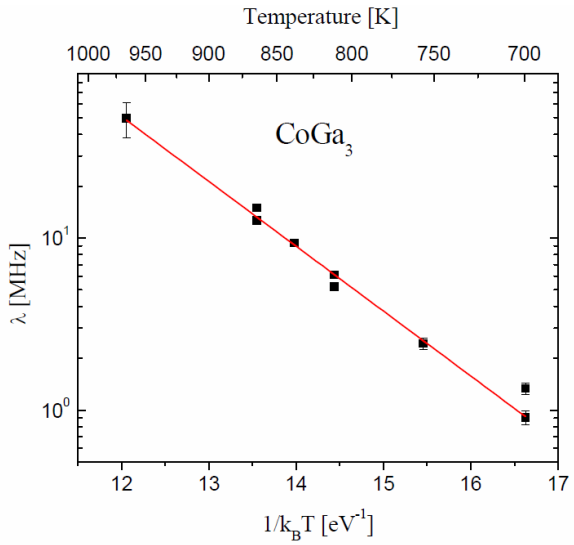

Fig. 4. Arrhenius plot of relaxation frequencies λ for PAC spectra in $CoGa_3$. The fitted activation enthalpy is 0.88(2) eV.

The activation-enthalpy previously found for $FeGa_3$ [14] was 1.86(8) eV, twice higher. The difference is attributed to semiconducting and metallic natures of FeGa3 and CoGa3, respectively. U. Haeussermann et al. showed via band-structure calculations that a rigid-band model applies to the two phases. The Fermi level in $FeGa_3$ happens to lie within a ~0.3 eV hybridization gap, making it semiconducting. The level for $CoGa_3$, with one additional electron, is above the gap, making it metallic. Presumably, conduction electrons in $CoGa_3$ are more effective at screening Coulomb-interactions, leading to a reduction in the activation-enthalpy for diffusion. This comparison suggests a potential, general difference between diffusion in metals and semiconductors. Haeussermann et al. also pointed out that the indium phase $RuIn_3$, with the same number of electrons as $FeGa_3$, is not a semiconductor, but instead a poor conductor, due to weaker interaction between the indium and transition-metal atoms and disappearance of the gap.

Relaxation activation-enthalpies determined in this work are collected in the following table, along with representative values of relaxation rates estimated at a common temperature of 860K.

Table 2. Activation-enthalpies for relaxation of quadrupole interactions for probes on sites In1 and In2 (or Ga2). Measurements were in the range 700-1000°C. Relaxation rates λ_1 and λ_2 at 860K were obtained by interpolating values from Arrhenius plots. Rates are characterized as "high" and "low" if rates were higher for one sample of a phase than another.

Phase	H_1 (eV)	λ_1 (MHz)	H_2 (eV)	λ_2 (MHz)	Relaxation rate and interpretation
FeGa3	-		1.86(8)	3.0	Ga-poor (from [14])
CoGa3	-		0.88(2)	15.	Ga-poor
IrIn3	1.26(8)	5.2	0.96(10)	12	low, initially In-rich
	0.97(10)	11.	0.65(5)	20	high, later In-poor
RhIn3	1.4(2)	2.5	0.81(5)	8	low (assume In-rich)
	0.74(2)	16.	0.63(2)	20.	high (assume In-poor)
RuIn3	0.6(2)	2.0	0.63(8)	1.7	low?
	0.4(1)	2.7	0.29(5)	3.8	high?

$IrIn_3$

Fig. 5 shows time-domain and frequency spectra for $IrIn_3$. Frequency spectra (right) are similar to those shown in Fig. 2 for $RuIn_3$, except that the fundamental frequencies of the two signals are accidentally coincident. Time-domain spectra were fitted with a superposition of two signals for probes on In2 and In1 sites, with static quadrupole-interaction parameters as given in Table 1. Measurements over the range 500-650°C exhibited dynamical-relaxation and the two spectral components were fitted using eq. 5.

Measurements on one sample gave unique insight into diffusion behavior and compositions. A sequence of nine measurements at various temperatures extended over two weeks. Relaxation rates in measurements 2-5 were relatively “low”, but shifted abruptly to rates a factor of three higher in measurements 6-9, designated “high” in Table 2. Figure 6 shows an Arrhenius plot of fitted relaxation rates for tracers starting on sites In1 and In2, with numbers 2-9 identifying the order in which the measurements were made. Note that measurement temperatures were varied up and down in random fashion, allowing one to observe that there was an abrupt change in behavior betw-

Defect and Diffusion Forum, vol. 120, 73-90, Advances in Mass and Thermal Transport in Engineering Materials III, ISSN print 1012-0386. https://s3.wp.wsu.edu/uploads/sites/893/2023/02/DSL_238-2022-a.pdf

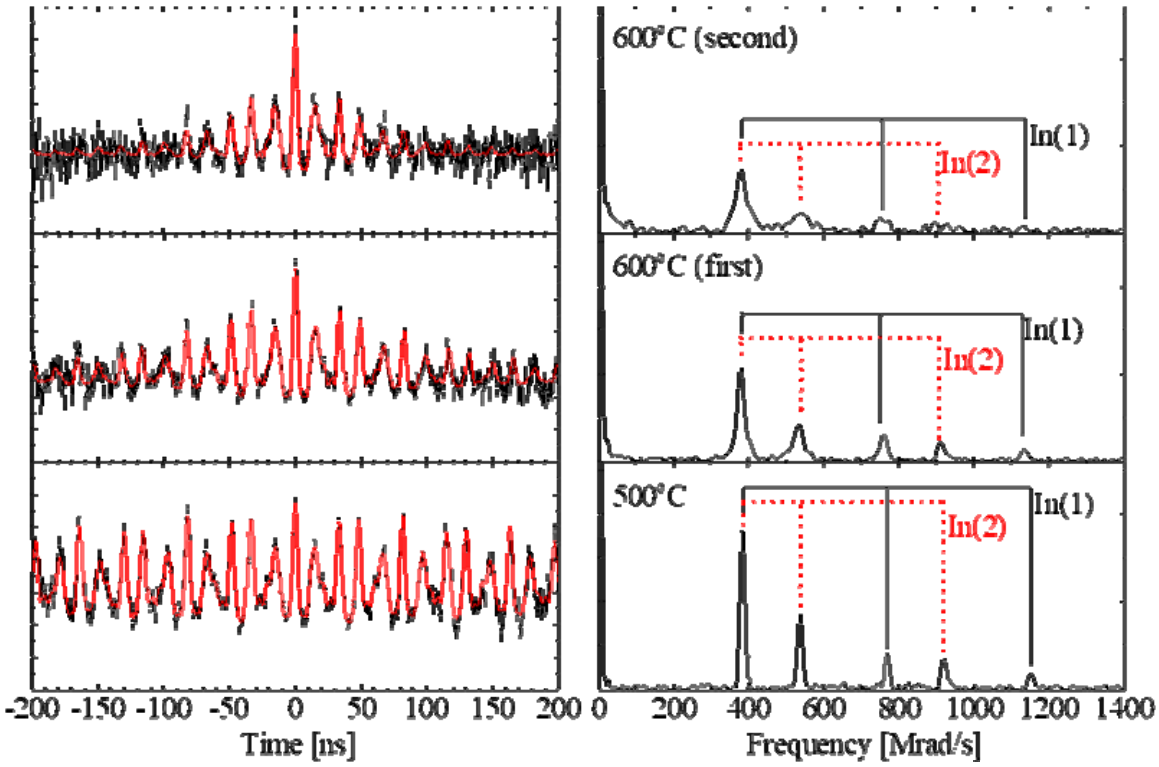

Fig. 5. PAC spectra of $IrIn_3$. Dynamical averaging is evident at 600°C as damping of time-domain spectra or as broadening of the frequency peaks. The middle and top spectra were runs 3 and 7 in the sequence shown in Fig. 6, both measured at 600°C. They show the shift in relaxation-rate from a "low" value to a "high" one discussed in the text. The shift is attributed to either evaporation of In from the sample or increased homogenization of the sample during multiple-day measurements at high-temperature.

een runs 5 and 6. Activation enthalpies were obtained by fitting data sets for each site with $\lambda = \lambda_0 \exp(H / k_B T)$, giving values H= 1.26 eV (In1) and 0.96 eV (In2) before the shift and 0.96 eV (In1) and 0.65 eV (In2) after the shift. Prefactors λ_0 were of order 5 x10^9 Hz, somewhat lower than expected values of 1-10 THz for a vacancy-diffusion mechanism.

Two alternative explanations are offered for the increase in relaxation-rate after days of measurements at high temperature. One needs to recognize that these phases are highly-ordered line-compounds. For the gallides, useful samples could only be made for Ga-poor samples because in Ga-rich samples, impurity ^{111}In activity was found to entirely dissolve in the small pools of liquid Ga-metal present (the next more Ga-rich phase), so that measurement of diffusional relaxation in the solid gallide phases were not possible. This was of course not a problem for indides since the tracer-probe is a host-element.

Because Ir, Rh and Ru have very high melting temperatures, homogeneity of the indide samples immediately after arc-melting appeared worse than in many other past studies. Some transition-metal may not have melted and mixed during the arc-melting and only gradually dissolved in the samples during experimental runs at high temperature. This would leave the 1:3 indide phase containing ^{111}In tracer initially richer in indium than expected based on the nominal composition. With increasing measurement time at high temperature, more transition-metal would become incorporated in the 1:3 phase through solid-state interdiffusion and reaction, increasing the volume fraction of the 1:3 phase at the expense of indium-metal.

Defect and Diffusion Forum, vol. 120, 73-90, Advances in Mass and Thermal Transport in Engineering Materials III, ISSN print 1012-0386. https://s3.wp.wsu.edu/uploads/sites/893/2023/02/DSL_238-2022-a.pdf

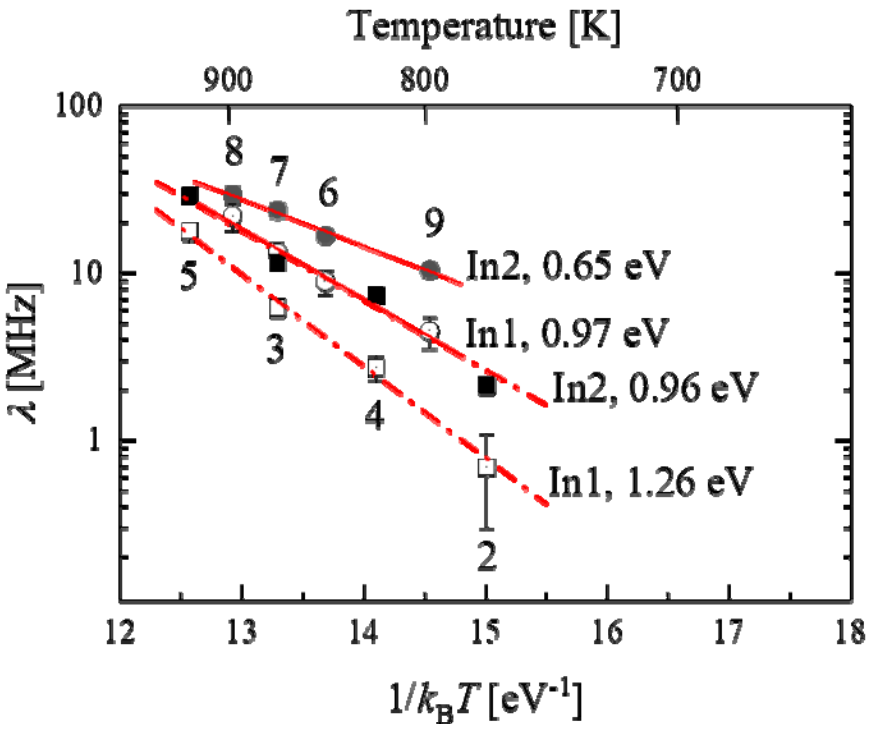

Fig.6. Arrhenius plots of relaxation frequencies for quadrupole-perturbation functions for tracer probes on In2 and In1 sites in an $IrIn_3$ sample. Numbers indicate the order of measurements. An abrupt increase in relaxation rate was observed between runs 5 and 6 in the sequence of measurements.

The amount of indium in the sample may likewise be decreasing owing to In-evaporation in the high-vacuum of the measurement ovens. The vapor-pressure of indium is much greater than of the transition-elements, so that all the evaporative mass-loss was indium. Mass-losses of several milligrams of indium from ~150 mg samples occurred over week-long measurements. Either homogenization or In-evaporation will reduce and eventually eliminate the volume fraction of indium metal, after which the single-phase 1:3 field will start to become In-poorer. The indium content of the 1:3 phase will decrease until the In-poor boundary composition is reached, after which the sample will consist of the 1:3 phase at fixed composition and a small volume fraction of the next, more In-poor phase, $IrIn_2$ [15]. Since vacancy mole-fractions within a phase always vary monotonically with sample composition, the In-vacancy mole-fraction will be greater at the In-poor than In-rich boundary composition. Assuming that diffusion occurs via an In-vacancy diffusion mechanism, the observed step-wise increase in jump-rate for $IrIn_3$ sample JB105 can be attributed to an increase in the vacancy mole-fraction due to either of these two processes. This same rationale was used to identify corresponding "high" and "low" rate samples of $RhIn_3$ and $RuIn_3$.

The abruptness of the increase in relaxation-rate between runs 5 and 6 in Fig. 6 attests to the narrow width of the $IrIn_3$ phase-field. While the overall sample is within a two-phase field having a mean composition just outside either boundary-composition of the phase, the equilibrium composition of the 1:3 phase remains anchored at either of the two boundary-compositions. Either incorporation of unmelted transition metal or evaporation of indium will reduce the average indium content of the sample. Starting from an In-rich composition, once the mean composition enters the single-phase field (say at 24.8 at.%), the composition evidently became rapidly In-poorer, sweeping across the compositional phase-field, until it reached the In-poorer phase boundary composition (say at 25.2 at.%). The phase henceforth remains at the In-poorer boundary composition.

In summary, the shift from low to high relaxation rate is consistent with decrease in In-metal content in the $IrIn_3$ phase of interest over time through either of two mechanisms described above. The abruptness is consistent with a narrow width of the phase-field, perhaps of the order of 0.1 at.%. The increase in mole-fraction of In-vacancies gives rise to an increase in relaxation consistent with a simple In-vacancy diffusion-mechanism. However, nominal compositions based on metal-masses that assumed homogeneous melting could not be trusted to give representative compositions of samples studied. Compositions based on metal-masses for all samples are listed in the Appendix for reference.

The same type of abrupt increase in relaxation rate, attributed to evaporation of indium, has been observed elsewhere. Fig. 7 from ref. [6] shows an Arrhenius plot of relaxation rates of ^{111}In/Cd tracers in the $L1_2$ indide $TmIn_3$. Originally In-rich (A), the sample lost indium through evaporation, making a transition (arrow) from a “slow” relaxation regime for the In-rich sample (A) to a "fast" relaxation regime for the In-poor (B) sample. The Arrhenius fits are nearly parallel and the abrupt factor-of-three increase in relaxation rate is attributed to an increased mole-fraction of In-vacancies at the In-poor boundary composition than at the In-rich boundary, similar to the present study.

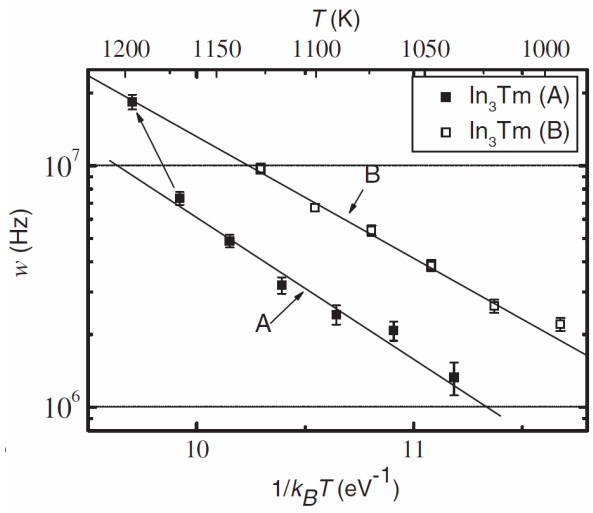

Figure 7. Relaxation rates for ^{111}In/Cd probes in a sample of $L1_2$ phase In_3Tm (reproduced from Fig. 2 right, ref. [6]). The sequence of measurements was up along the lower line (A) and then down along the upper line (B) after a transition between 1170K and 1195K shown by the arrow.

Table 2 shows that activation-enthalpies for sites In1 and In2 are lower in the “high” rate regime than in the “low”. The difference of 0.3 eV can be qualitatively attributed to the formation-enthalpy for In-vacancies in the two cases, as explained in the discussion below. There is a greater component of constitutional vacancies in the “high-rate” regime, whereas vacancies in the low-rate regime must be thermally activated. Presumably, activation-enthalpies for migration are about the same for both regimes, so that the difference in activation enthalpies can be understood as part of the effective formation enthalpy of In-vacancies, or about 0.3 eV per vacancy in $IrIn_3$.

$RhIn_3$

Fig. 8 shows PAC spectra for a $RhIn_3$ sample. With increasing temperature, the empirical exponential relaxation leads to damping in the time-domain and broadening of peaks in the frequency-spectra. Frequency spectra look different than for $RuIn_3$ in Fig. 2 because fundamental frequencies of signals for tracer probes on sites In1 and In2 accidentally overlap, as they did for $IrIn_3$ in Fig. 5. Fitted quadrupole interaction parameters are given in Tab. 1.

Defect and Diffusion Forum, vol. 120, 73-90, Advances in Mass and Thermal Transport in Engineering Materials III, ISSN print 1012-0386. https://s3.wp.wsu.edu/uploads/sites/893/2023/02/DSL_238-2022-a.pdf

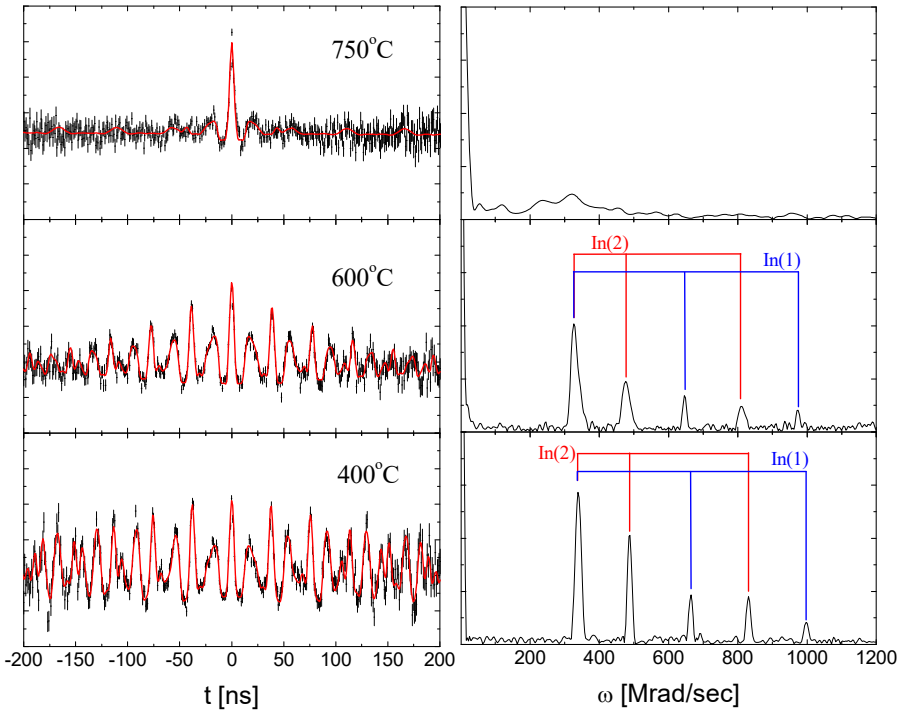

Fig. 8. PAC spectra measured in $RhIn_3$. Damping increases with temperature. The In2 signal has greater damping than the In1 signal, as can be seen by broader peaks of the second and third harmonics of the In2 signal than of the In1 signal in the frequency spectrum at 600°C.

Perturbation functions for tracers on In1 and In2 sites in time-domain spectra were fitted with exponential damping-functions in the same way as for $IrIn_3$. Relaxation-frequencies are shown in Fig. 9 for a sample exhibiting high relaxation-rates and in Fig. 10 for one exhibiting low rates.

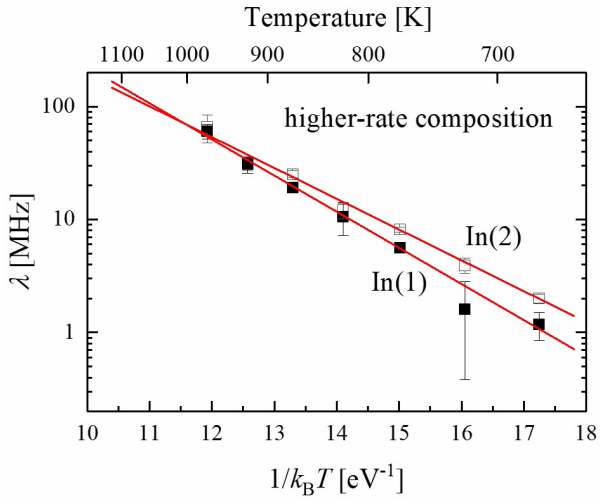

Fig. 9. Arrhenius plot of relaxations for a $RhIn_3$ sample having a high relaxation rate.

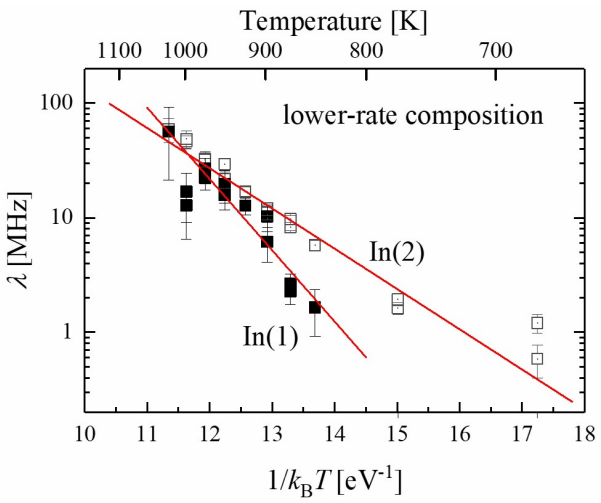

Fig. 10. Arrhenius plot of relaxations for a $RhIn_3$ sample having a low relaxation rate.

Similar to $IrIn_3$, relaxation-rates for tracer atoms starting on In2 sites are greater at lower temperatures than for those starting on In1 sites and the activation enthalpies are lower. However, for low-rate $RhIn_3$, the activation enthalpy for In1 relaxation is greater by 0.6 eV than for In2, and there appears to be a crossover in magnitudes of relaxation frequencies at 1000K, with tracers on In2 sites having greater relaxation rates at lower temperatures. However, for the high-rate sample,

the difference is only 0.1 eV. These differences are discussed below in terms of site-preferences of daughter Cd-probes and of In-vacancies..

$RuIn_3$

Arrhenius plots of relaxation rates of In1 and In2 signals in $RuIn_3$ are shown for a high-rate sample in Fig. 11 and low-rate sample in Fig. 12. The relaxation behavior is qualitatively similar to those of $IrIn_3$ and $RhIn_3$, although not as well defined.

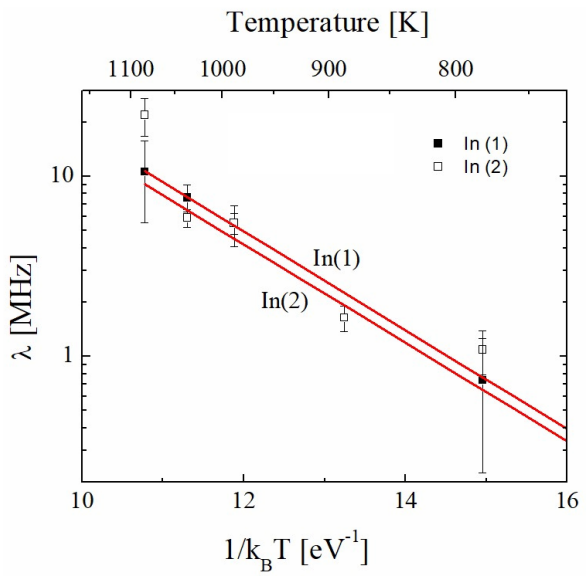

Fig. 11. Arrhenius plot of relaxation for a $RuIn_3$ sample having a high relaxation rate.

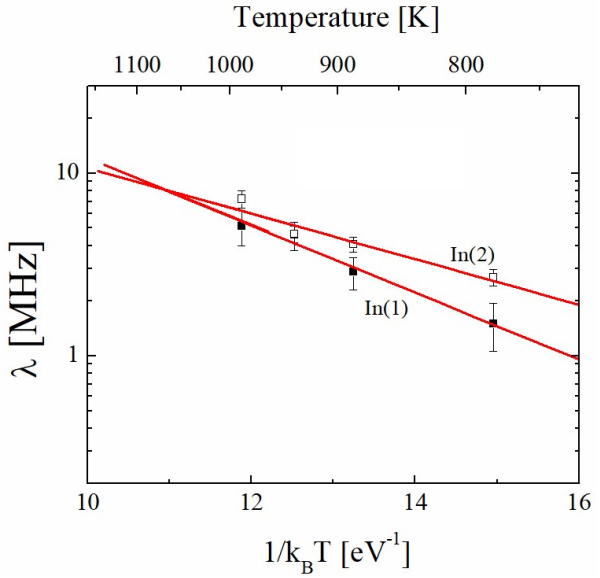

Fig. 12. Arrhenius plot of relaxation for a $RuIn_3$ sample having a low relaxation rate.

Microscopic Jump-Processes

Lattice-parameters of the two gallide and three indide phases are very similar, apart from overall volume-scaling. Haeussermann et al. enumerated distances to close-neighbors of type-2 and type-1 sites [13]. After scaling distances by the cube-root of the atomic volumes, Table 3 gives the close neighbor distances from In1 and In2 sites in $IrIn_3$.

Table 3. Neighboring sites of In1 and In2 sites in tetragonal $IrIn_3$, giving numbers of equivalent neighbors, distances, and descriptions of neighbor destination-sites in jumps (confer Fig. 1). Two distances are given when there are equivalent sites that are essentially identical. Jump labels used in an earlier study of $FeGa_3$ [14] are given in parentheses.

Site		Jump to...	Jump label	Distances (A)	Locations of destination sites
In1	8	In2	12	3.150+ 3.249	Surrounding cube of 8 In2 atoms
	2	In1	11	3.641	In1 in next cubes above and below
In2	1	In2	22a (2)	3.062	Short diagonal across rhombus
	4	In1	21	3.150+ 3.249	Centers of four touching In2 cubes
	2	In2	22b (3,3')	3.466+ 3.723	On tetragonal axis above and below
	4	In2	22c (1)	3.816	Four closest In2 atoms in basal plane

For the analysis of relaxation for $FeGa_3$ in ref. [14] and for $CoGa_3$ in the present study, ^{111}In tracer atoms only occupied Ga2 sites, and destination sites to which tracers could jump are labeled 22a, 22b and 22c in the table (previously labelled 2, (3+3'), and 1, respectively, in ref. [14]).

Defect and Diffusion Forum, vol. 120, 73-90, Advances in Mass and Thermal Transport in Engineering Materials III, ISSN print 1012-0386. https://s3.wp.wsu.edu/uploads/sites/893/2023/02/DSL_238-2022-a.pdf

Assuming a simple In-vacancy diffusion mechanism, the ratio of relaxation frequencies of tracer atoms in phases of "high" and "low" relaxation rate at a given temperature gives insight into the ratio of mole-fractions of In-vacancies in the two types of phase. As described above, it is believed that samples having high and low relaxation rates have compositions at the opposing phase boundaries. Depending on precise compositions and their distances from the 25 at.% stoichiometric composition, there may be constitutional and/or thermally activated In-vacancies. Qualitatively, ratios of relaxation-frequencies at 860K are found to equal ~2 in IrIn3 and ~4 in $RhIn_3$ (Table 2). Without more information about actual boundary compositions (which might be very close to each other and to the stoichiometric composition), one cannot say more.

Discussion

Differences in efg relaxation. Table 2 shows significant differences between activation-enthalpies for probes starting on In1 and In2 sites, and for sample compositions giving high or low relaxation rates. The results are clearer for $IrIn_3$ and $RhIn_3$. Ultimately, the relaxation comes from atomic jumps of probe atoms during the nuclear lifetime of the PAC level leading to changes in electric field gradients. In previous studies of nuclear relaxation in $L1_2$ and Al_4Ba phases described in the introduction, there was a unique relationship between physical jumps and changes in efgs. In addition, there was only a single kind of jump. In the present work, there are two diffusion sublattices, many jumps between and among the two types of sites, each and its own migration enthalpy, and changes in efgs associated with each jump. A comprehensive analysis of the observed relaxation is unattainable. However, one can still try to understand why, for example, the activation-enthalpies for relaxation of probes starting on In1 or In2 sites are so different for low-rate $RhIn_3$ (Fig. 10) and the origin of the differences between activation-enthalpies in high-rate and low-rate samples. Two phenomena are considered that help explain the observations.

1. Site-preference of the daughter Cd-solute. While site-fractions of the parent In-probe must be in the ratio 1:2 up to the time of transmutation, daughter Cd-probes will in general have a site-preference for one site or the other. Cd-probes will repartition within the first few jumps, driving the site-fraction ratio towards a new equilibrium distribution given by

$$f_2 / f_1 = 2\exp\left(-(H_2 - H_1)/k_B T\right), \qquad (6)$$

in which H_i is the site-enthalpy of the Cd-tracer atom on site i. It will take 1-2 jumps of the tracers to establish the new equilibrium distribution. For a relaxation rate of ~10 MHz, this means that the first 100-200 ns of a spectrum may be disturbed by a nonequilibrium partition of the tracer atoms.

Spectra were fitted to a sum of signals for the two sites given in eq. 5, with each term containing its relaxation factor $\exp(-\lambda t)$. Suppose for point of argument that the daughter Cd-probe preferred site In1 over site In2 (H_2 more positive than H_1), so that the equilibrium value of the amplitude of the In1 signal *increased* over time in the first jump or two. The spectral component for site In1 will therefore become relatively larger over a time-interval of 1-2 jumps, while the component for site In2 will become smaller. When fitting using eq. 5, λ_1 will be fitted smaller (less decrease) than the relaxation due solely to jumps and λ_2 will be fitted larger (greater decrease). The overall effect is to increase λ_2, reduce λ_1, even if there were no differences in migration-rates Qualitatively, this is the behavior observed clearly for "low-rate" $RhIn_3$ (see Fig. 10), and also for "low-rate" $IrIn_3$.

2. Mole-fractions of vacancies on the two sites. The $IrIn_3$ (or $FeGa_3$) structure is close-packed and diffusion almost certainly takes place via an In-vacancy mechanism. For the tracer atom to

jump via one of the processes listed in Table 3, there must be a vacancy at the destination site. The physical jump-rate $w_{a\to b}$ of a tracer atom from sublattice *a* to sublattice *b* depends on the activation enthalpy to jump (migration enthalpy) and on the mole-fraction of vacancies at sites on the destination-sublattice *b*, $[V_b]$,

$$w_{a\to b} = w_{0a}[V_b]\exp(-H^{mig}_{a\to b}/k_BT), \tag{7}$$

in which $H^{mig}_{a\to b}$ is a migration enthalpy barrier and w_{0a} is a jump-attempt frequency. The ratio of mole-fractions of vacancies on the two sublattices is given by an expression analogous to eq. 6,

$$[V_1]/[V_2] = \exp\left(-(H^V_1 - H^V_2)/k_BT\right). \tag{8}$$

If, for example, vacancies have less positive site-enthalpies on In1 sites, then the mole-fraction of vacancies on sublattice In1 will be greater, thereby increasing the jump-rate of Cd-probes to sublattice In1. (The vacancies can readily maintain their equilibrium distribution despite Cd-atom jumps by exchanging with In-atoms on the other sublattice.)

Putting it all together, the ratio of jump-rates in opposite directions between In1 and In2 sites for a single jump-process in Table 3 is then

$$\frac{w_{2\to1}}{w_{1\to2}} = \frac{w_{02}}{w_{01}}\frac{f_2}{f_1}\frac{[V_1]}{[V_2]}\exp\left(-(H^{mig}_{2\to1} - H^{mig}_{1\to2})/k_BT\right). \tag{9}$$

The site-preferences of probe atoms and/or vacancies can help to explain the greater relaxation observed for probes starting on In2 sites.

3. High-rate vs. low-rate samples. High-rate samples of the indide phase are believed to have In-poor boundary compositions, and therefore more In-vacancies. From Table 2, the ratio of relaxation-rates for high- and low-rate samples of $IrIn_3$ and $RhIn_3$ at 860K is of order 2-4, suggesting that vacancy mole-fractions are greater by the same factors. Activation enthalpies for high-rate samples are typically 0.3 eV lower than for low-rate samples. Assuming that high-rate samples have a mixture of both constitutional and thermal vacancies, the 0.3 eV enthalpy difference can be taken to be a portion of the effective vacancy formation enthalpy in the indide phases.

Gallides vs. indides. Activation enthalpies for the two gallides can be compared with those for indides with a high rate of relaxation because of the presence of relatively high numbers of vacancies in both cases. There is a greater number of jump processes open to tracers in the indides than gallides because the probes occupy both In1 and In2 sites (see Table 3). The relaxation activation-enthalpy for site Ga2 in metallic $CoGa_3$ (Ga-poor, 0.88 eV) is 0.25 eV greater than for sites In2 in comparable "high-rate" $IrIn_3$ and $RhIn_3$ (In-poor, 0.63 eV). This may be due to the smaller number of jump-processes possible in the gallides.

Relationship to diffusivity in indium metal. Since the indide phases are 75% indium, it is natural to compare the diffusivity of probes in the indide phases with that in pure indium metal. As determined by positron-annihilation [22], the activation enthalpy for self-diffusion in indium metal, 0.81(5) eV, is equal to the sum of activation enthalpies for vacancy-formation, 0.54(3) eV, and migration, 0.27(4) eV, The appropriate comparison is with relaxation data for "low"-rate samples of $IrIn_3$ and $RhIn_3$, which presumably have fewer, if any, constitutional In-vacancies (indium metal has none). From Table 2, the mean enthalpy of relaxation for tracers on sublattice In2 in "low"-rate samples is 0.88 eV, in excellent agreement with 0.81 eV for In-metal. However, the mean enthalpy

for tracers jumping from sublattice In1 in "low"-rate samples is 1.33 eV, suggesting that there may be a strong site-preference of Cd-daughters for the In1 sublattice. The activation enthalpy in "high"-rate alloys, for which there is a significant role of constitutional vacancies, and therefore perhaps no effective formation enthalpy, averages ~0.73 eV for both sites and both phases, much greater than the 0.27 eV migration enthalpy in indium metal alone. This may indicate that interactions between indium and transition-metal atoms increase the migration enthalpy relative to indium metal. Or it may indicate that there are appreciable amounts of both thermally-activated and constitutional In-vacancies at the In-poorer (high-rate) boundary compositions, so that the 0.73 eV value represents the migration enthalpy as well as a portion of the vacancy formation enthalpy.

Summary

Diffusional relaxation of nuclear quadrupole interactions was measured for ^{111}In/Cd tracer atoms in indide and gallide phases having the $FeGa_3$ crystal structure. There are two inequivalent In(Ga) sites, and relaxation was monitored by fitting quadrupole perturbation-functions for the two sites using an exponential damping *ansatz*. Measurements were made in the slow-fluctuation regime, with jump-frequencies less than quadrupole-interaction frequencies. Relaxation rates were found to be greater for In2 sites than In1 sites. This was attributed in part to differences in site-preferences of the Cd-daughter tracer atoms and/or differences in site-preferences of vacancies. After decay of In into Cd, 1-2 jumps are need to reach the new equilibrium distribution of atoms and defects in the phases. This leads to disturbance of the time-domain PAC spectra over a time of order 100 ns, inverse of the mean relaxation frequency.

The phases are line-compounds. Samples prepared to have compositions at the opposing phase boundaries were found to exhibit "high" or "low" relaxation rates. One sample of IrIn3 also exhibited an abrupt transition from "low" to "high" rate in the course of a series of measurements. This was explained by assuming a simple In-vacancy diffusion mechanism with higher efg relaxation rates in samples that have higher mole-fractions of constitutional vacancies in the phase of $FeGa_3$ structure, that is, in more In-poor samples. Activation enthalpies for relaxation of quadrupole interactions in the indide phases are compared and the activation enthalpy for relaxation in low-rate IrIn3 and RhIn3 samples was found to be close to the activation enthalpy for diffusion in metallic indium.

Appendix

Nominal compositions of indides samples. 100-150 mg samples of metal foils were rapidly arc-melted and then resolidified under argon within 1-2 seconds. There was often significant mass-loss attributed to evaporation of metals during the melting. It was assumed that evaporative mass-losses of transition-metals and indium were proportional to their vapor pressures at a temperature of order 1800^{o}C. Owing to the enormously greater vapor-pressure of indium, all mass-losses were attributed to indium. Table A1 gives nominal compositions of samples before melting and compositions after melting assuming that mass-losses were of indium. Also given is an indication as to whether the observed relaxation rate observed via PAC was qualitatively "low" or "high", and whether the observed relaxation rate was consistent with the mean composition after melting, assuming good homogenization during melting. For five out of the eight samples listed, the rate was inconsistent with the nominal composition after melting, pointing to poor homogenization of these high melting-point transition metals.

Defect and Diffusion Forum, vol. 120, 73-90, Advances in Mass and Thermal Transport in Engineering Materials III, ISSN print 1012-0386. https://s3.wp.wsu.edu/uploads/sites/893/2023/02/DSL_238-2022-a.pdf

Table A1. Transition-metal compositions of samples studied.

Phase	Before melt at.%	After melt at.%	Relaxation rate	Sample
$IrIn_3$	22.5	27.6	low → high *a*	JB105
	20.1	20.5	low *a*	RN089
	27.0	32.8	low	PS002
$RhIn_3$	21.9	25.5	high *a*	RN084
	27.2	28.7	low	RN074
	27.1	29.1	low	PS001
$RuIn_3$	22.0	22.5	high?	RN090
	27	35.9	low?	RN091

a. Assuming that a high relaxation-rate is associated with a greater mole-fraction of In-vacancies, the inferred relaxation rate is consistent with the composition after melting.

References

[1] H. Mehrer, *Diffusion in Solids: Fundamentals, Methods, Materials, Diffusion-Controlled Processes*, Springer Series in Solid-State Sciences, vol. 155, 2007.

[2] M.O. Zacate, A. Favrot, G.S. Collins, Atom *movement in In_3La studied via nuclear quadrupole relaxation*, Physical Review Letters 92 (2004) 225901; *erratum* Physical Review Letters 93 (2004) 49903.

[3] G. S. Collins, A. Favrot, L. Kang, D. Solodovnikov and M.O. Zacate, *Diffusion in intermetallic compounds studied using nuclear quadrupole relaxation*, Defect and Diffusion Forum 237-240, (2005) 195-200.

[4] G.S. Collins, A. Favrot, L. Kang, E.R. Nieuwenhuis, D. Solodovnikov, J. Wang, M.O. Zacate, *PAC probes as diffusion tracers in solids*, Hyperfine Interactions 159 (2005) 1-8.

[5] X. Jiang, M.O. Zacate, G.S. Collins, *Jump frequencies of Cd tracer atoms in $L1_2$ lanthanide gallides*, Defect and Diffusion Forum 289-292 (2009) 725-732.

[6] G.S. Collins, X. Jiang, J.P. Bevington, F. Selim and M.O. Zacate, *Change of diffusion mechanism with lattice parameter in the series of lanthanide indides having $L1_2$ structure*, Physical Review Letters 102, 155901 (2009).

[7] M. Lockwood, B. Norman, R. Newhouse, G.S. Collins, *Comparison of jump frequencies of ^{111}In/Cd tracer atoms in Sn_3R and In_3R phases having the $L1_2$ structure (R= rare earth)*, Defect and Diffusion Forum 311 (2011) 159-166.

[8] Q. Wang and G.S. Collins, *Nuclear quadrupole interactions of ^{111}In/Cd solute atoms in a series of rare-earth palladium alloys*, Hyperfine Interactions 221 (2013) 85-98.

[9] E.R. Nieuwenhuis, M.O. Zacate and G.S. Collins, *Simultaneous measurement of tracer jump frequencies on different sublattices in Ga_7Pd_3 using PAC*, Defect and Diffusion Forum 264 (2007) 27-32.

[10] F. Selim, J.P. Bevington and G.S. Collins, *Diffusion of ^{111}Cd probes in Ga_7Pt_3 studied via nuclear quadrupole relaxatio*n, Hyperfine Interactions 178, 87-90 (2007).

[11] S. Lage and G.S. Collins, *Motion of cadmium tracer atoms in $Al_{11}R_3$ phases (R= La, Ce, Pr)*, Defect and Diffusion Forum 289-292, 755-761 (2009).

[12] R. Newhouse, S. Cawthorne, G.S. Collins, M.O. Zacate, *Diffusion of tracer atoms in Al_4Ba phases studied using perturbed angular correlation spectroscopy*, submitted to Crystals (2022).

[13] U. Haeussermann, M. Bostroem, P. Viklund, O. Rapp, T. Bjoernaengen, *$FeGa_3$ and $RuGa_3$: Semiconducting Intermetallic Compounds*, J. Solid State Chemistry 165 (2002) 94.

[14] R. Newhouse, G.S. Collins, M.O. Zacate, *Site occupation of indium and jump frequencies of cadmium in $FeGa_3$* Hyperfine Interact. 238 (2017) 137.

[15] C.E.T. White and H. Okamoto, eds., *Phase Diagrams of Indium Alloys and Their Engineering Applications*, ASM International, Materials Park, OH, 1992.

[16] Xiangyu Yin, *Indium solubility in α-gallium and gallium-indium eutectic alloys studied using PAC*, MS thesis, Washington State University, 2011 (unpublished).

[17] Randal G. Newhouse, *Atomic jump frequencies in intermetallic compounds studied using perturbed angular correlation of gamma rays*, PhD dissertation, Washington State University, 2012 (unpublished).

[18] C.E.T. White, H. Okamoto, eds., *Phase Diagrams of Indium Alloys and Their Engineering Applications*, ASM, Materials Park, OH, 1992.

[19] G.S. Collins, *Nonstoichiometry in line compounds,* Journal of Materials Science 42 (2007) 1915-1919.

[20] A.R. Arends, C. Hohenemser, F. Pleiter, H de Waard, L. Chow, R.M. Suter, *Data reduction methodology for perturbed angular correlation experiments*, Hyperfine Interctions 8, 191-213 (1980).

[21] G. Schatz, A. Weidinger, *Nuclear Condensed Matter Physics: Nuclear Methods and Applications*, John Wiley, New York, 1996.

[22] W. Weiler, H.-E. Schaefer, *Vacancy formation in indium investigated by positron lifetime spectroscopy*, J. Phys. F: Metal Physics 15 (1985) 1651.